Journal of Nuclear Materials 390–391 (2009) 267–273

Contents lists available at ScienceDirect

Journal of Nuclear Materials

journal homepage: www.elsevier.com/locate/jnucmat

The impact of divertor detachment on carbon sources in JET L-mode discharges

S. Brezinsek [a,*], A.G. Meigs [b], S. Jachmich [c], M.F. Stamp [b], J. Rapp [a,d], R. Felton [b], R.A. Pitts [e], V. Philipps [a], A. Huber [a], R. Pugno [f], G. Sergienko [a], A. Pospieszczyk [a] and JET-EFDA contributors[1]

JET-EFDA, Culham Science Centre, Abingdon, Oxon OX14 3DB, UK
[a] *Institut für Energieforschung-Plasmaphysik, Forschungszentrum Jülich,[2] Association EURATOM-FZJ, Germany*
[b] *EURATOM/UKAEA Fusion Association, Culham Science Centre, Abingdon, Oxon OX14 3DB, UK*
[c] *LPP-ERM/KMS,2 Association EURATOM-Belgian State, Belgium*
[d] *FOM-Rijnhuizen,2 Association EURATOM-FOM, The Netherlands*
[e] *CRPP-EPFL, Association EURATOM-Confdration Suisse, CH-1015 Lausanne, Switzerland*
[f] *Association EURATOM-Max-Planck-Institut für Plasmaphysik, D-85748 Garching, Germany*

ARTICLE INFO

PACS:
52.70.Kz
52.40.Hf
52.25.Vy
52.55.Fa
33.20.Lg

ABSTRACT

Hydrocarbon injection experiments have been performed to investigate the chemical sputtering yield of carbon-fibre composites at elevated temperatures ($T_{surface} \simeq 500$ K) and detached plasma conditions in the JET outer divertor. A plasma scenario in L-mode with the outer strike-point positioned on the load bearing septum replacement plate was developed to detach the outer divertor leg and to provide the strong recombining target plasma. The operational window was explored in a set of discharges with strong deuterium puffing into the private-flux region. Langmuir probes showed a clear roll-over in the ion flux up to complete plasma detachment at the target plate during the density ramp of the discharge. Paschen recombination line analysis shows strong volume recombination with electron temperatures below 2.0 eV prior to the appearance of a radiation instability – an X-point Marfe. A strong reduction of the intrinsic *CD* photon flux was observed under these conditions, whereas local CD_4 injection still led to *CD* photon flux emission. This provides conclusive evidence for a reduction of the hydrocarbon flux and the chemical sputtering under detached plasma conditions.

1. Introduction

Detached divertor operation is mandatory on ITER to reduce the expected high heat loads on plasma-facing components (PFCs) – in particular on the divertor target plates made of carbon-fibre composites (CFC) and/or tungsten – to manageable levels [1]. Divertor detachment, thus the retraction of the plasma from the target plate caused by pressure loss, appears at low electron temperature/recombining plasma operation at high electron densities [2]. The impact energy of fuel ions drops below the threshold for physical sputtering so that for CFC targets, only chemical sputtering remains as a source for the impurity influx close to the strike-point areas [3].

Chemical sputtering can be described as a function of ion energy, ion flux and surface temperature [4], though uncertainties with respect to data interpretation and extrapolation to detached plasma conditions exist. Recent experiments in ASDEX Upgrade and DIII-D at low surface temperatures ($T_{surface} \simeq 350$ K) showed a reduction of the intrinsic hydrocarbon flux and the chemical sputtering yield under detached conditions in comparison to attached conditions in high density plasmas [5–7]. Chemical sputtering at these low $T_{surface}$ is caused by ion induced desorption of hydrocarbon radicals and not by thermal emission of hydrocarbon radicals enhanced by radiation damage as described in [4]. But the latter mechanism will dominate the chemical sputtering in ITER at the expected higher target temperatures. A reduced carbon source is favourable for ITER operation to minimise the carbon migration and the subsequent appearance of co-deposited fuel in carbon layers. Carbon which is necessary to radiate in the divertor to obtain/maintain the divertor detachment is eroded in the scrape-off layer (SOL) spatially away from the strike-zone on the target plate [3].

An experiment at JET with detached outer divertor leg has been performed to investigate the sputtering yield at $T_{surface} \simeq 500$ K, closer to the maximum temperature of chemical sputtering which is then determined by thermal emission of hydrocarbon radicals

* Corresponding author. Addresses: Institut für Energieforschung-Plasmaphysik, Forschungszentrum Jülich, Association EURATOM-FZJ, Germany; JET-EFDA, Culham Science Centre, Abingdon, Oxon OX14 3DB, UK.
E-mail addresses: sebastijan.brezinsek@jet.efda.org, s.brezinsek@fz-juelich.de (S. Brezinsek).

[1] See annex of J. Pamela et al., Fusion Energy 2002 (Proceedings of the 19th International Conference, Lyon, 2002), IAEA, Vienna.

[2] Partners in the Trilateral Euregio Cluster (TEC).

0022-3115/$ - see front matter © 2009 Published by Elsevier B.V.
doi:10.1016/j.jnucmat.2009.01.100

enhanced by radiation damage. Quantification of the chemical sputtering is done in situ with spectroscopy on the hydrocarbon break-up product *CD* in combination with local CD_4 injection [5] into the near outboard SOL through a gas injection module with a single hole. This experiment focuses on both the exploitation of steady-state detached divertor operation with carbon PFCs and the determination of the carbon erosion under these conditions.

2. Experimental set-up and plasma scenario

A plasma scenario in lower single-null magnetic configuration with the outer strike-point (OSP) fixed on the centre of the load bearing septum replacement plate (LBSRP) – depicted in Fig. 1(a) – was developed to detach the outer divertor leg at the local injection location with the aid of strong deuterium fuelling. The exper-

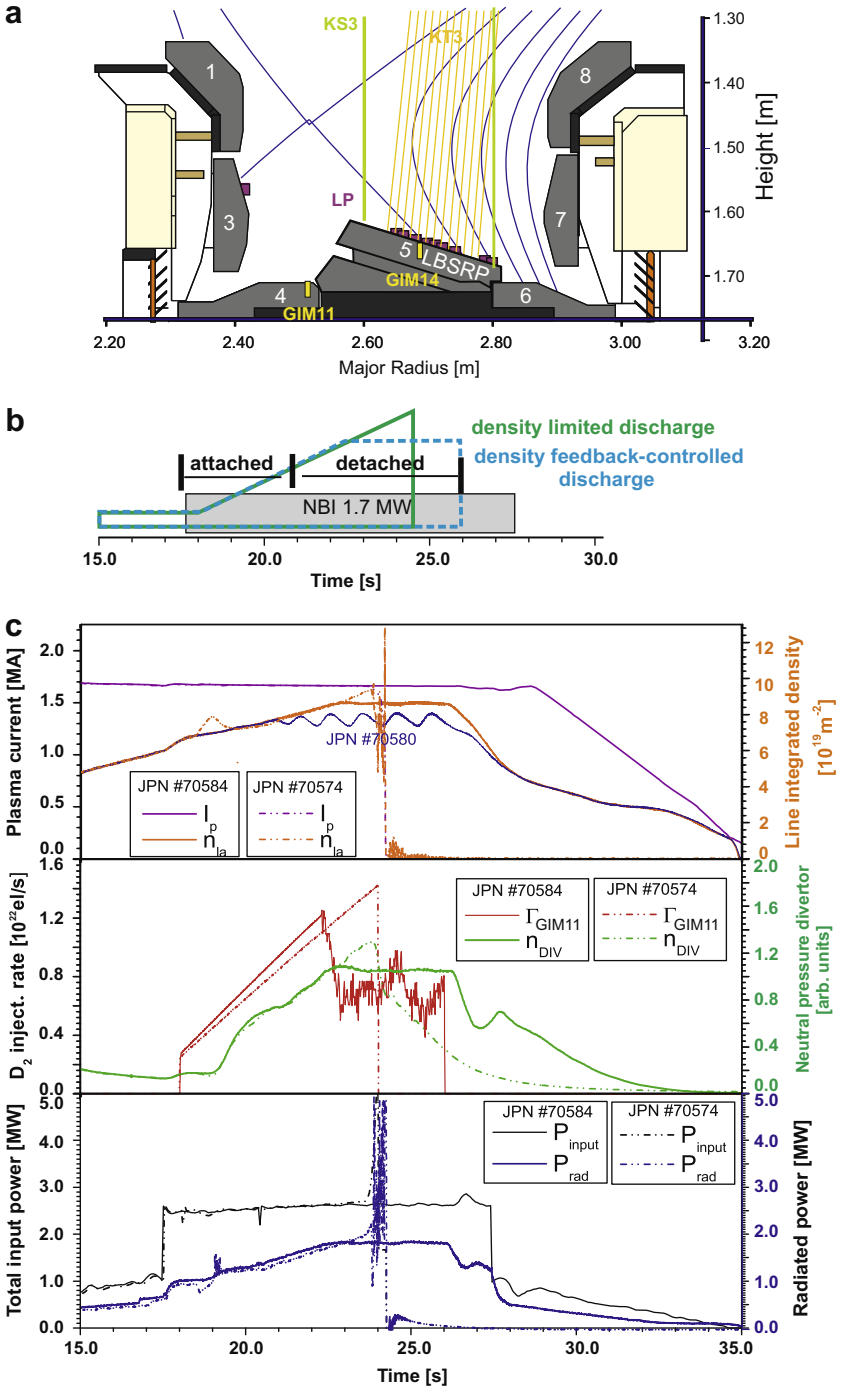

Fig. 1. (a) Magnetic configuration and diagnostic coverage in the JET MKII-HD divertor. The outer strike-point is positioned on the gas injection location (GIM14) which is embedded in the load bearing septum replacement plate (divertor tile 5). (b) Schematic time setting of the central density and the additional heating in the two pulse types applied in the experiment: density ramp-up (—) and density feedback-controlled discharge (---). In the latter the density was steadily increased to typically 90% of the density limit and than feedback-controlled with the aid of deuterium gas injection. (c) Time traces of global parameters for transient and steady-state detached divertor operation: central density and plasma current (top), D_2 injection rate and neutral pressure (middle), and total input power and radiated power (bottom). In steady-state detached operation, the set point for feedback control was set to 92% of the maximum achievable density. Discharge #70580 with a control level of 80% of the maximum density showed an oscillation between attached and (semi-)detached plasma operation.

iment was performed in L-mode with moderate additional heating power ($P_{aux} = 1.8$ MW) by neutral beam injection (NBI) at high toroidal magnetic field ($B_t = 2.7$ T) and moderate plasma current ($I_p = 1.8$ MA) to ensure operation below the L–H transition threshold. A magnetic configuration with medium triangularity ($\delta = 0.39$) and large distance between the separatrix and the top of the machine (30 cm) is chosen to reduce the plasma-wall interaction in the main chamber. The poloidal length of the inner divertor leg with a maximum distance of 8.5 cm between the X-point and the inner strike-point was short in comparison with the outer leg with 13 cm distance between X-point and tile 5 – the LBSRP. This short poloidal distance actually reduces the ease with which the inner divertor detaches, in contrast to more balanced divertor geometries at JET, where the inner target is often completely detached, even for moderate densities in L-mode plasmas. The configuration was optimised for both access to detached divertor plasma operation (transient and feedback-controlled) and the in situ calibration of the eroded hydrocarbon flux using spectroscopy and local gas injection. The operational window for feedback-controlled outer divertor detachment was explored in a set of discharges with strong deuterium puffing into the private-flux region (PFR). Deuterium was injected through a circumferential gas injection module located in the base plate of the inner divertor (labelled GIM11) and ramped-up (with maximum fuelling rates up to 1.4×10^{22} D/s) to the density limit (Fig. 1(b)). The transition from an attached to a detached divertor plasma was determined by the roll-over of the ion flux Γ_{D^+} measured with the aid of a set of Langmuir Probes (LP) embedded in the LBSRP and the appearance of deuterium volume recombination monitored spectroscopically.

The increase of the central density and the neutral pressure in the subdivertor with the D_2 injection ramp as well as the power balance between total input and radiated power is shown in Fig. 1(c) for the representative discharge #70574. Several reproducible pulses were performed to vary diagnostic settings for best characterisation of this transient regime. The discharge terminates rapidly in a density limit disruption for radiated powers beyond a radiated fraction of 80%. Steady-state detached divertor operation with a flat-top phase of about 6 s was achieved by real-time feedback control on the edge density with the injection rate as actuator. The set point for the density feedback was typically fixed to 92% of the density limit. Time traces of global parameters are depicted for the representative discharge #70584 in Fig. 1(c), too. Oscillation between detached and attached divertor operation (#70580) occurred if the gain factor was set to high and the density set point to close to the attached regime. This oscillation was used to compare attached and detached plasma operation in a single discharge.

A number of diagnostics are used to characterise the cold and dense divertor plasma. The tile embedded LP (KY4D [8]) and Paschen/Balmer recombination spectroscopy (KT3) provide electron temperature T_e and electron density n_e, radiated powers are obtained with the divertor bolometry system (KB5 [9]) and the divertor neutral density n_D is supplied by a subdivertor neutral pressure gauge (KT5P). In situ the hydrocarbon flux Γ^{CD} and the deuterium recycling flux Γ^{D} are obtained with the aid of divertor spectroscopy (KS3 [4]) and local CD_4 injection (GIM14). Fig. 1(a) illustrates the detection coverage of the toroidally separated diagnostics in one toroidal plane of the divertor.

3. Characterisation of the detached outer divertor plasma

The degree of detachment (DOD) provides a normalisation criterion for the increase of the ion flux with upstream plasma density, at constant power flux into the edge plasma, compared with the expected dependence in high recycling case ($\Gamma_{D^+} \sim \overline{n_e^2}$) [10]. Fig. 2 shows the time evolution of both *DOD*, related either to the *separatrix* (DOD^{sep}) or *integral* (DOD^{int}) ion fluxes onto the LBSRP, during the density ramp of pulse #70574 normalised to the start of the high recycling phase at 19.2 s. The LP at the OSP showed a clear Γ_{D^+} roll-over during the density ramp at $t = 20.7$ s, indicating the beginning of the detachment process and a linear increase of both DOD^{sep} and DOD^{int}. The faster rise of DOD^{sep} implies that the detachment starts at the separatrix and extends to the SOL. At $t = 22.5$ s the SOL at the LBSRP is almost completely detached ($DOD > 3$ [10]), and Marfe formation [2] at the X-point gradually sets in. The corresponding change of the peaked profile at the target ($T_e = 50$ eV and $n_e = 1.2 \times 10^{20}$ m^{-3}) to an almost flat profile with significantly reduced peak values down to $T_e < 10$ eV and $n_e < 4 \times 10^{19}$ m^{-3} is depicted in Fig. 3(a).

Detachment is mandatory but not sufficient for the appearance of volume recombination in the divertor. Significant volume recombination sets in at T_e below 5 eV [2,11]. Here, volume recombination was detected in the outer leg using analysis of the Paschen and/or Balmer recombination lines [11]. The Stark broadening of Paschen high-n lines with $n = 7$–9 provides the n_e distribution at the LBSRP shown in Fig. 3(b). Using both the Paschen continuum and the line ratios of the $n = 10$–12 lines, $T_e < 2.0$ eV is found at the OSP (Fig. 3(b)) at $t = 22.5$ s. The time evolution of the Paschen–ϵ line (Fig. 3(c)) shows that the volume recombination (and the low T_e plasma) begins at the OSP at $t = 20.7$ s and extends

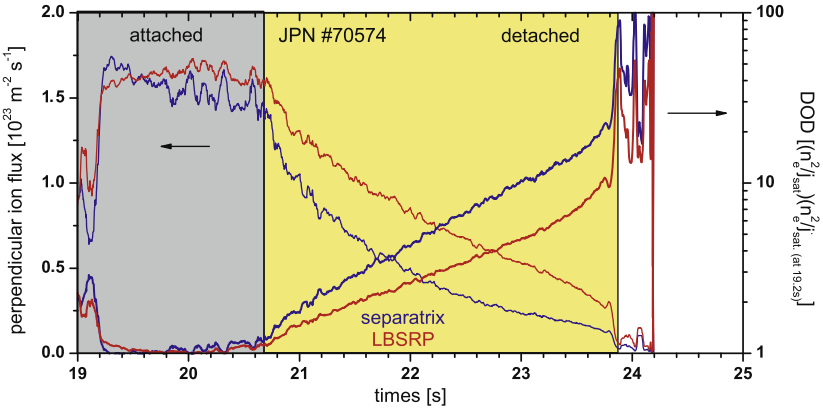

Fig. 2. The degree of detachment (DOD) and the deuterium ion flux (Γ_{D^+}) at the outer divertor target plate was measured with an array of embedded Langmuir probes during the density ramp-up discharge. The constant DOD prior to $t = 20.7$ s indicates the high recycling regime. The sudden decrease of Γ_{D^+} at the separatrix and the corresponding linear increase of DOD^{sep} show the start of the detachment which begins at the outer strike-point and expands in time over the LBSRP. DOD^{int} is related to the integrated ion flux to the LBSRP.

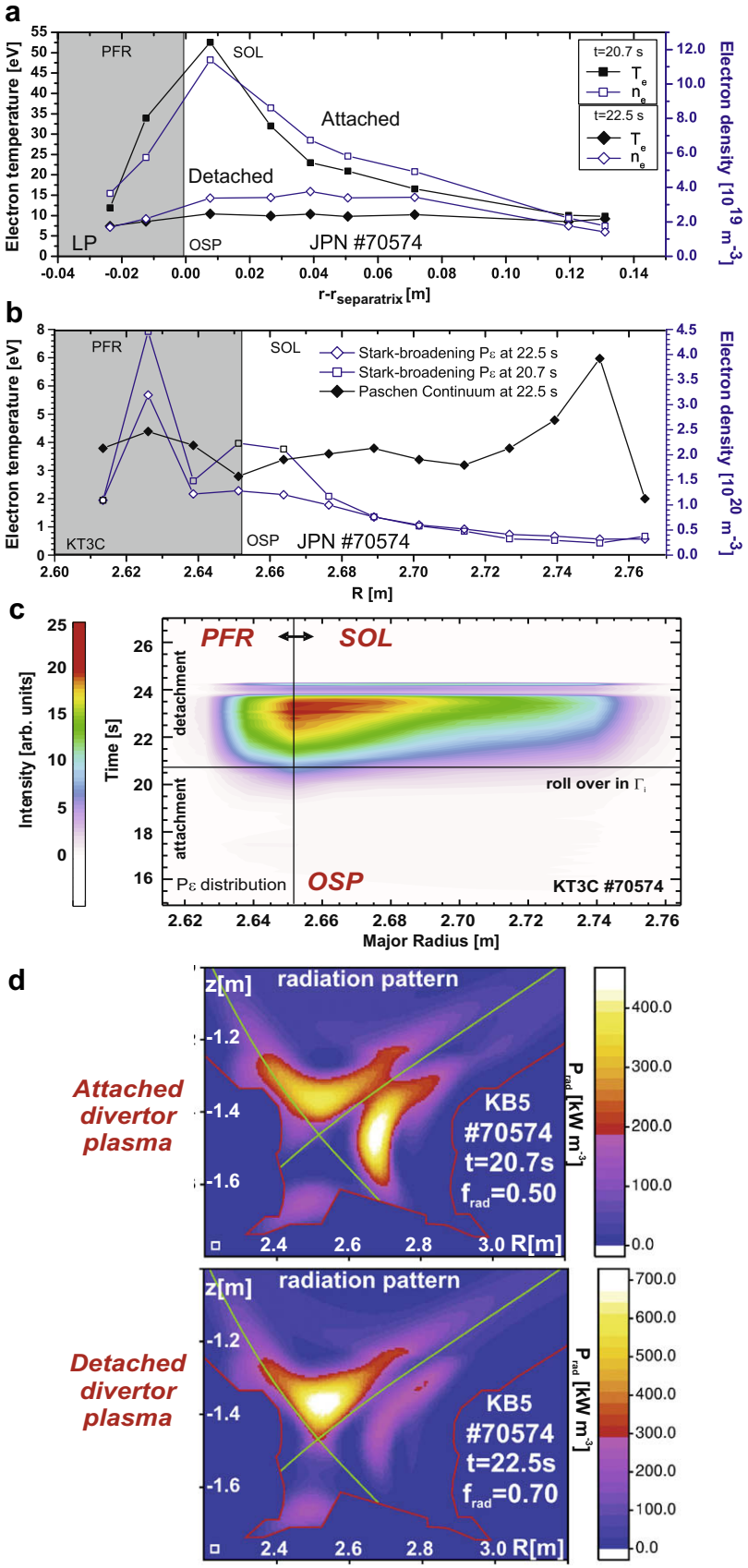

Fig. 3. Plasma characterisation in the outer divertor leg during high recycling ($t = 20.7$ s) and detachment ($t = 22.5$ s). (a) Electron temperature and electron density profiles at the target plate deduced from Langmuir probe measurements. (b) Electron density profiles obtained from line broadening analysis of high-n Paschen lines. Electron temperature profile deduced from the Paschen recombination continuum analysis. (c) Time evolution of Paschen–ϵ line emission. The private-flux region (PFR), the outer strike-point (OSP) location and the scrape-off layer (SOL) are indicated. (d) Radiation pattern in the divertor under attached plasma (top) and detached plasma conditions (bottom).

into the SOL as time and density increase, confirming that partial detachment in this magnetic configuration occurs first near the OSP.

This spectroscopic observation of intense deuterium volume recombination is an irrefutable indicator of a low T_e plasma in the outer divertor and is entirely consistent with the strong reduction in the local Γ_{D^+} to the target plate. And yet, although the LP temperature profile (Fig. 3(a)) collapses across tile 5, it is never much lower than $T_e \simeq 10$ eV. This situation is extremely reminiscent of observations reported on TCV [12] where the standard divertor geometry is similar to the JET configuration used here. Despite the strong outer target detachment seen in low power, density ramp experiments, the T_e at the target plate, measured by tile embedded LPs, never fell to the low values expected in a detached plasma. The latter is also characterised by strong parallel temperature gradients in the X-point vicinity, followed by an extended convective region of low T_e down to the target. The high measured T_e is therefore very likely due to a small population of electrons from further upstream, travelling collisionless to the target LPs.

The total radiation reconstructions shown in Fig. 3(d) are also consistent with a picture in which the rather open nature of the

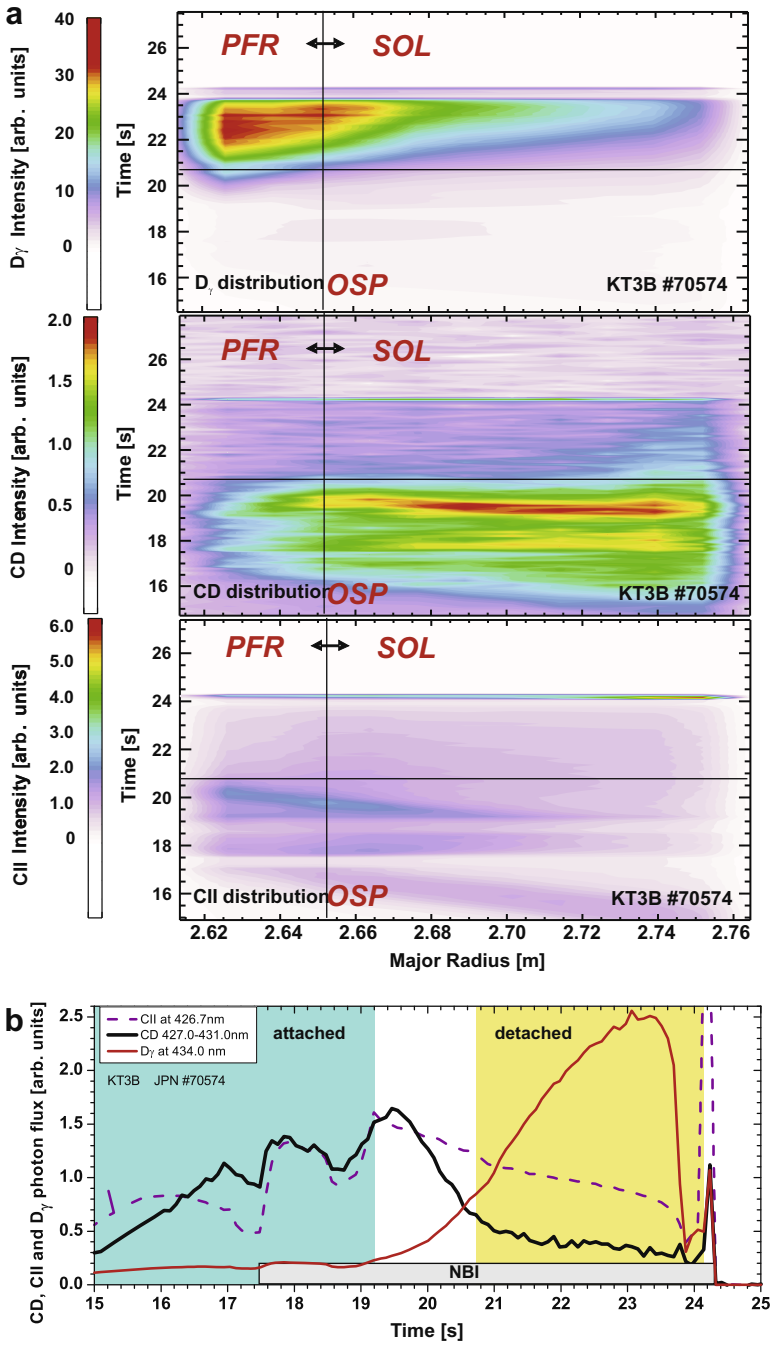

Fig. 4. (a) Spatial distribution of D_γ, *CD* A–X band and *CII* emission in the outer divertor during the density ramp-up with transition from attached to detached plasma regime. The auxiliary heating (NBI) was applied from $t = 17.5$ s on until the density limit disruption occurred. (b) Time evolution of the integrated photon fluxes of D_γ and both carbon transitions during the density ramp-up discharge. The steep rise of D_γ and the strong decrease in *CD* starts at $t = 19.2$ s when the ion flux shows the roll-over and volume recombination sets in.

chosen divertor configuration allows carbon impurities and deuterium neutrals to readily escape the outer target region. Radiation then occurs preferentially in the higher T_e plasma in the X-point vicinity, leading to enhanced power exhaustion (and stronger detachment) as heat fluxes arriving from the main SOL encounter the strongly radiating region.

4. Impact of divertor detachment on the hydrocarbon flux

A direct comparison between attached and detached divertor operation is made in a single shot to study the impact of detachment on the carbon impurity source distribution and strength. Both the reduced impact energy and the increase in the total incident particle flux (ions and atoms) induced by detachment have an impact on the chemical sputtering. Fig. 4(a) shows the spatial distribution at the outer target of the *CD* Gerö band, indicator of the intrinsic hydrocarbon flux, and the *CII* line (426.7 nm), indicator of the total carbon flux from chemical and physical sputtering, and ϕ_{D_γ}, indicator of the deuterium recycling flux and incident ion flux [5] for ionising dominated plasmas or of volume recombination for low temperature recombining plasmas. The corresponding integrated photon fluxes $\phi_{CD}^{intrinsic}$ and $\phi_{CII}^{intrinsic}$ are given in Fig. 4(b) together with the D_γ photon flux ϕ_{D_γ}. The D_γ light pattern shows a strong increase due to a significant contribution from recombination starting at the OSP close to the roll-over of Γ_{D^+} and extending to the SOL. In contrast, the light pattern of both carbon transitions show a strong reduction coincident with the D_γ increase. Surprisingly the maximum emission of the *CD* Gerö band in the high recycling regime is separated a few cm spatially away from the OSP into the SOL. The maximum emission of the *CII* line is, however, well correlated with the location of the OSP in both the attached and the high recycling phases, suggesting that in addition to chemical sputtering, physical sputtering also contributes to C^+. Note that the strong radiation in the X-point region might contribute to the emission pattern of carbon and deuterium in the two innermost KT3 chords.

The strong reduction of $\phi_{CD}^{intrinsic}$ by about a factor 5 between $t = 19.5$ s and 22.5 s can be divided into two phases in which the first one (steep slope) occurs in the high recycling phase ($t = 19.5$–20.7 s) and the second one (flat slope) in the detached phase ($t > 20.7$ s). The *CD* light pattern is consistent with this division: the first reduction occurs all over the target in the SOL, whereas during the second, the remaining *CD* is located close to the ionisation front. This *CD* light source diminishes as the *DOD* increases. The $\phi_{CII}^{intrinsic}$ shows a slow and less pronounced reduction to half the initial value in the detached phase with a slope similar to that found for the second phase of $\phi_{CD}^{intrinsic}$ decay.

To calibrate the hydrocarbon flux, CD_4 was injected at the separatrix through GIM14 located toroidally between two modules of tile 5 into discharges with density feedback control. Fig. 5(a) shows the time evolution of the spectral range between 425.0 nm and 437.0 nm – including both carbon transitions and D_γ in a discharge with oscillation between divertor attached and detached phases and pulsed hydrocarbon injection. The *CII* line and the *CD* Gerö band behave anti-correlated to the emission of D_γ confirming the reduction of intrinsic carbon light emission at recombining plasma conditions. The extrinsic photon flux $\phi_{CD}^{extrinsic}$ from *CD* radicals originating from the break-up of injected CD_4 could clearly be detected with the integral line-of-sight of KS3 of 20 cm diameter centred on the injection valve to ensure a large coverage of the emission cloud

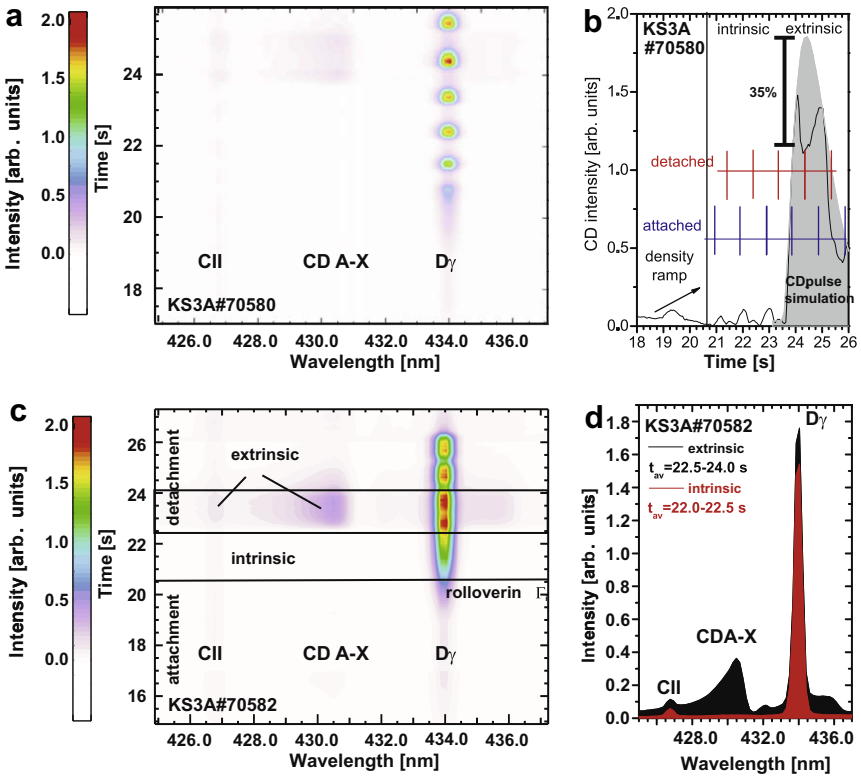

Fig. 5. (a) The intrinsic *CD* A–X band emission, which is substantial under attached plasma conditions, is strongly suppressed when detached and recombining plasma conditions with $T_e < 2$ eV are reached. This can be seen in both, during the density ramp at the beginning of the discharge and during the plasma oscillation between attached and detached operation in feedback control. (b) The time trace of the *CD* A–X band head shows alternation in the light emission with alternation of the plasma regime. CD_4 injection leads to significant emission of extrinsic *CD* A–X band emission in both plasma regimes though the reconstruction of the injected gas pulse shows a slightly lower photon efficiency for recombining plasmas. (c) Local CD_4 injection into a density feedback-controlled discharge and detached outer divertor leg. (d) Time averaged emission spectrum of D_γ, *CD* A–X band, and *CII* at 426.7 nm prior to and during the local CD_4 injection in the detached divertor leg.

(Fig. 1(a)); a loss of photons out of the observation volume under detached conditions cannot be fully excluded. Since only pulsed injection was possible and the pulse length extends for times longer than the attached–detached oscillation frequency, the pulse shape is accounted in the analysis as depicted in Fig. 5(b). The extrinsic *CD* A–X photons in both phases are detectable, but photon efficiencies in the recombining (detached) and ionising (attached) plasma differ by 35%.

The absolute quantification of the effective inverse photon efficiency $\left[\frac{D}{XB}\right]^{CD_4\rightarrow CD}_{A^2\Delta\rightarrow X^2\Pi}$ for the complete electronic transition [4] in the detached phase to $\left[\frac{D}{XB}\right]^{CD_4\rightarrow CD}_{A^2\Delta\rightarrow X^2\Pi} = 45 \pm 22$ was performed in discharge #70582 with constant density during the CD_4 injection (Fig. 5(c)). Fig. 5(d) shows two spectra taken prior and during the hydrocarbon injection in the steady-state detached phase. The intrinsic *CD* A–X band is at the detection limit of the spectroscopic system (KS3), whereas the extrinsic *CD* A–X band is clearly detectable. There is no increase of D_γ due to the CD_4 injection detectable, thus, the local injection is minor perturbing the local detached plasma conditions.

The corresponding effective inverse photon efficiency for the high density attached plasma amounts 30 ± 15. The slight difference of $\left[\frac{D}{XB}\right]^{CD_4\rightarrow CD}_{A^2\Delta\rightarrow X^2\Pi}$ in attached and detached plasmas cannot account for the strong reduction of $\phi^{intrinsic}_{CD}$ by a factor 4.8 observed during density ramp (Fig. 4(b)). This suppression of $\phi^{intrinsic}_{CD}$ is then caused indeed by the reduction of the hydrocarbon particle flux $\Gamma^{intrinsic}_{CD_4}$ by more than a factor 3.1 in the detached plasma in comparison to the attached plasma, thus, by the reduction of the chemical erosion source.

5. Summary and conclusion

The experimental observations at JET can be summarised as followed:

- Outer divertor detachment with recombining plasma established.
- CD_4 injection leads to significant extrinsic *CD* A–X photon flux in detached plasma conditions.
- The inverse photon efficiency in detached plasma conditions is slightly higher in comparison to attached plasmas.
- Strong reduction of the intrinsic hydrocarbon flux as soon as D_γ starts to rise and the ion flux measured by Langmuir probes shows roll-over.
- Almost complete suppression of chemical sputtering with detached outer leg on the LBSRP and recombining deuterium plasma with $T_e < 2.0$ eV.

This experiment confirms the reduction of the chemical sputtering yield under detached and recombining plasma conditions close to the maximum surface temperature of carbon erosion. The reduction is caused by both an energetic threshold for the damage processes which causes the chemical sputtering at these surface temperatures ($T_{surface} > 500$ K) and the high incident flux of ions and atoms at plasma temperatures below 2 eV.

Acknowledgements

This work, supported by the European Communities under the contract of Association between EURATOM/FZJ, was carried out within the framework of EFDA. The views and opinions expressed herein do not necessarily reflect those of the European Commission. This work was done in the frame of the EU Task force for Plasma-Wall Interaction and the International Tokamak Physics Activity (task: DSOL-2).

References

[1] G. Federici et al., Nucl. Fus. 41 (12R) (2001) 1967.
[2] P.C. Stangeby, The Plasma Boundary of Magnetic Fusion Devices, Institute of Physics Publishing, Bristol, 2000.
[3] A. Kirschner et al., J. Nucl. Mater. 363–365 (2007) 91.
[4] J. Roth et al., Nucl. Fus. 44 (L21) (2004).
[5] S. Brezinsek et al., J. Nucl. Mater. 363–365 (2007) 1119.
[6] S. Brezinsek et al., Phys. Scripta T128 (2007) 40.
[7] A. McLean et al., J. Nucl. Mater. 363–365 (2007) 86.
[8] S. Jachmich et al., J. Nucl. Mater. 363–365 (2007) 1050.
[9] A. Huber et al., J. Nucl. Mater. 363–365 (2007) 365.
[10] A. Loarte et al., Nucl. Fus. 38 (3) (1998) 331.
[11] ADAS. <http://adas.phys.strath.ac.uk>.
[12] R.A. Pitts et al., J. Nucl. Mater. 290–293 (2001) 940.